Polymer Chemistry

PAPER

View Article Online
View Journal | View Issue

Cite this: *Polym. Chem.*, 2016, **7**, 7514

Increased hydrophobic block length of PTDMs promotes protein internalization†

Coralie M. Backlund,[a] Federica Sgolastra,[a] Ronja Otter,[a] Lisa M. Minter,[b,c] Toshihide Takeuchi,[d] Shiroh Futaki[d] and Gregory N. Tew*[a,b,c]

Received 13th September 2016,
Accepted 8th November 2016

DOI: 10.1039/c6py01615d

www.rsc.org/polymers

The plasma membrane is a major obstacle in the development and use of biomacromolecules for intracellular therapeutic applications. Protein transduction domains (PTDs) have been used to overcome this barrier, but often require covalent conjugation to their cargo and can be time consuming to synthesize. Synthetic monomers can be designed to mimic the amino acid moieties in PTDs, and their resulting polymers provide a well-controlled platform to vary molecular composition for structure–activity relationship studies. In this paper, a series of polyoxanorbornene-based synthetic mimics, inspired by PTDs, with varying cationic and hydrophobic densities, and the nature of the hydrophobic chain and degree of polymerizations were investigated *in vitro* to determine their ability to non-covalently transport enhanced green fluorescent protein into HeLa cells, Jurkat T cells, and hTERT mesenchymal stem cells. Polymers with high charge density lead to efficient protein delivery. Similarly, the polymers with the highest hydrophobic content and density proved to be the most efficient at internalization. The observed improvements with increased hydrophobic length and content were consistent across all three cell types, suggesting that these architectural relationships are not cell type specific. However, Jurkat T cells showed more variation in uptake between polymers than with the other two cell types. These results provide important design parameters for effective delivery of biomacromolecules for intracellular delivery applications.

Introduction

The plasma membrane plays a crucial role in cell survival, acting as a selectively penetrable barrier limiting large macromolecules from entering the cytoplasm.[1] As the field of molecular biology expands, investigation of intracellular processes is often hampered by the inability of biomacromolecules, such as proteins and antibodies, to efficiently and selectively cross the cell membrane.[2] The use of protein transduction domains (PTDs), sometimes referred to as cell penetrating peptides (CPPs), to facilitate the delivery of large biological cargo can be used to overcome this barrier.[2–4] PTDs are generally short, cationic protein segments with the ability to traverse the phospholipid bilayer.[5] The first protein discovered with this ability was the HIV-1 TAT protein.[6,7] Subsequent studies found that TAT's ability to translocate the membrane was largely due to the arginine rich domain between residues 48–60.[8] Guanidinium groups, such as those present in polyarginine, have since been shown to be important in facilitating translocation.[9,10] Through studying TAT and several other naturally occurring PTDs, along with their structural derivatives, it became apparent that secondary protein structure and peptide based backbones are not essential requirements for efficient cellular uptake, but that charge content is critical with guanidine functionality being particularly efficient.[8,10–14] Consequently, a large number of highly charged, cationic PTD mimics (PTDMs) have been reported.[15–22]

More recently, addition of a hydrophobic domain has been shown to improve membrane transduction activity.[23] Examples of this are N-terminal stearylation/acylation of polyargine,[24] and the use of supramolecular, hydrophobic counter ions,[9,25,26] which improve both membrane affinity and cellular internalization. Inherently amphiphilic CPPs, such as penetratin, have also provided a source of inspiration for chimera mimics like Pep-1.[27–29] Additionally, aromaticity has also been shown to play a role in membrane interactions and translocation;[30–32] oligoarginine activity has been enhanced with the use of aromatic counter ions, and with the incorporation of tryptophan or phenylalanine in the peptide sequences.[33–36] Given the importance of aromatic amino acids

[a]*Department of Polymer Science & Engineering, University of Massachusetts, Amherst, MA 01003, USA. E-mail: tew@mail.pse.umass.edu*
[b]*Department of Veterinary & Animal Sciences, University of Massachusetts, Amherst, MA 01003, USA*
[c]*Molecular & Cellular Biology Program, University of Massachusetts, Amherst, MA 01003, USA*
[d]*Institute for Chemical Research, Kyoto University, Uji, Kyoto 611-0011, Japan*
†Electronic supplementary information (ESI) available. See DOI: 10.1039/c6py01615d

in membrane proteins and their unique interactions with the bilayer, it was proposed that aromatic side chains would make better activators than other hydrophobic amino acids, given equal relative hydrophobicity.[10,37,38,42]

We have previously reported the synthesis and preliminary investigations of oxanorbornene based guanidinium rich polymer mimics of polyarginine, which have shown higher membrane activity compared to their polyarginine counterparts.[39–41] Aromatic groups were studied and the role of hydrophobicity has been further explored for protein delivery using PTDMs.[42,43,47] More specifically, constitutional macromolecular isomers[45] have been used to investigate the importance of sequence segregation for cellular internalization and protein delivery, instilling the importance of a distinct hydrophobic domain.[44] In this paper, we have designed and characterized eight different block-copolymer PTDMs inspired by polyarginine and amphiphilic peptides to deliver protein *via* non-covalent complexes into HeLa cells, as well as two hard to transfect cell types, Jurkat T cells, and hTERT mesenchymal stem cells (MSCs), thus providing critical information regarding the importance of hydrophobicity in PTDM delivery systems.

Polymer mimics offer distinct advantages over peptide derivatives of PTDs in that they are functionally and structurally versatile. In our previously reported synthetic approach, we achieved well-defined PTDMs with control over the spatial arrangement of positive charges and hydrophobic groups.[41–47] These molecules were obtained using ring-opening metathesis polymerization (ROMP), a technique well known for its highly controlled nature, functional group tolerance, and rapid polymerization times. Here, we extend this platform to access a series of block copolymers with precise hydrophobic and cationic content and density. Control over monomer hydrophobic content also enables deconvolution of side chain hydrophobicity from the hydrophobicity imparted by the polymer backbone. Using HPLC to determine the relative hydrophobicity of the monomers allows us to relate the hydrophobic content of each polymer, in terms of length, with their ability to deliver cargo.

Attachment of cargo *via* covalent linkage is often required for efficient use of PTDs.[5,48,49] The polymers studied here are able to form stable, non-covalent complexes with their associated cargos that are then internalized into cells.[40] In the context of promoting fundamental studies, non-covalent interactions are preferred due to their simplicity, delivery efficiency, and minimization of labor.[50] To evaluate the ability of these protein-containing complexes to enter cells, enhanced green fluorescent protein (EGFP) was chosen as a cargo. Flow cytometry was used to determine both the percentage of cells that receive the cargo, as well as the extent of uptake in the cells of interest. Additionally, cell viability was assessed after treatment, though very little toxicity was seen from any of the polymer–protein complexes.

In general, we found that a high density of cationic charge with a longer hydrophobic block led to higher levels of uptake. While some hydrophobic content threshold was required, the overall hydrophobic density seemed to have less of an impact than cationic density or length of the hydrophobic block on the ability of the block copolymers to efficiently internalize cargo. From this it has been hypothesized that increased hydrophobic block length creates a more stable interaction with the cargo protein. Similar results were found across all three cell types suggesting that this trend is applicable to all ROMP-based oxanorbornene block copolymers. The structure–activity study of these PTDMs provides guidance for building polymers that enable more efficient delivery of cargo, such as proteins, as tools to probe intracellular pathways.

Materials and methods

PTDM synthesis

Monomers and polymers were synthesized according to previously established procedures.[39,41,47] Details are reported in the ESI.† Briefly, the *exo* Diels–Alder adduct of maleic anhydride and furan was ring-opened with the desired alcohol to introduce the first substituent. A second alcohol was then added using EDC coupling. Five monomers were created in total: Methyl-Guanidine (**MeG**), di-guanidine (**dG**), di-methyl (**dMe**), methyl-phenyl (**MePh**), and di-phenyl (**dPh**). The desired polymers were obtained by ring-opening metathesis polymerization using Grubb's third generation catalyst in dichloromethane. After polymerization, the Boc groups were removed with a 1 : 1 solution of trifluoroacetic acid and dichloromethane. The final products were purified by dialysis against RO water and recovered by lyophilization.

Characterization

Reverse phase HPLC. Water and acetonitrile were each prepared with 0.1% trifluoroacetic acid for the liquid phase. Monomers were prepared at 5 mg mL^{-1} in DMSO, which also served as the flow marker. Samples were loaded onto a C8 reverse phase column held at room temperature and run at a gradient of 100% water to 100% acetonitrile over 60 minutes. Each sample was followed by 15 minutes of equilibration back to water prior to loading of the next sample.

Dynamic light scattering. $\mathbf{dPh_{10}}$-*b*-$\mathbf{dG_5}$, $\mathbf{MePh_{10}}$-*b*-$\mathbf{dG_5}$, and $\mathbf{dMe_{10}}$-*b*-$\mathbf{dG_5}$ were dissolved in DMSO and brought to a final concentration of both 5 mg mL^{-1} and 2.5 mg mL^{-1}. Samples were subjected to dynamic light scattering (DLS) at 10 degree intervals between 30 and 90 degrees. An exponential decay was fit to the data to calculate the R_h values of the polymers. Exponential fits can be found in the ESI.†

Protein delivery

Suspension cells. Jurkat T cells, a human T lymphocyte leukemia cell line (clone E6-1, ATCC TIB-152), were grown in RPMI 1640 supplemented with 10% (v/v) FBS, L-glutamine, Non Essential Amino Acids (NEAA), Na-buterate, 100 U mL^{-1} penicillin, and 100 U mL^{-1} streptomycin at 37 °C, 5% CO_2 and were passaged 24 hours before treatment. Polymers were mixed with 2 μg of EGFP at a ratio of 20 : 1 polymer to protein

and allowed to complex for 30 minutes. Jurkats were harvested and resuspended in fresh complete media and placed into a 12 well plate at 4×10^5 cells per mL. PTDM–protein complexes were applied drop-wise into each well. Cells were treated for 4 hours, then washed 3 times with 20 U mL^{-1} heparin in PBS before being suspended in 0.2% BSA FACS buffer and stained with 7-AAD. EGFP internalization and viability were assessed by flow cytometry using a BD LSR-II (BectonDickinson, Franklin Lakes, NJ). EGFP fluorophores were excited at 488 nm, and fluorescence was measured at 530 nm. The fluorescence signal was collected for 10 000 cells and viable cells were gated on to obtain a histogram of fluorescence intensity per cell. Live cells were assessed for their median fluorescence intensity (MFI) and their total positive shift in fluorescence (% positive). Internalization and delivery was repeated in three independent experiments. Statistical analysis was performed using the one way ANOVA and Tukey *post hoc* test to determine significance between polymers.

Adherent cells. HeLa (human) and hTERT mesenchymal stem cells (MSCs) were grown at 37 °C with 5% CO_2 in DMEM supplemented with 10% (v/v) FBS, 100 U mL^{-1} penicillin, and 100 U mL^{-1} streptomycin. Cells were plated at 5×10^4 cells per mL in a 12 well plate 48 hours before treatment for FACS analysis or 1×10^6 cells in a 35 mm glass bottom plate for CLSM. Polymers were mixed with 2 μg of EGFP at a molar ratio of 20 : 1 polymer to protein and allowed to complex for 30 minutes during which cells were aspirated and covered in fresh complete media. PTDM–protein complexes were applied drop-wise into each well. After 4 hours of treatment, cells were aspirated and trypsinized with 0.1% trypsin, then treated with complete media to bind excess trypsin. Cells were then washed 3 times with 20 U mL^{-1} heparin in PBS before being suspended in 2% FBS FACS buffer and stained with 7-aminoactinomycin D (7-AAD). Similar to the Jurakts, EGFP internalization and viability were assessed by flow cytometry under the same conditions.

Confocal laser scanning microscopy. HeLa cells were seeded at 10^6 cells per 2 mL of α-MEM with 10% FBS on 35 mm glass bottom plates and 10^5 cells per mL on 12-well plates 48 hours prior to treatment and cultured at 37 °C and 5% CO_2. Polymer was complexed with 2 μg of protein at a ratio of 20 : 1 polymer to protein for 30 minutes, during which the cells were aspirated and covered in fresh complete media. Cells were treated for 4 hours with the polymer protein complexes in a total volume of 1 mL α-MEM with 10% FBS. Before imaging, cells were washed three times with cold media and covered in 1 mL fresh cold α-MEM with 10% FBS. Cells were imaged using a FV300 CSLM Olympus IX81 microscope at 60×.

Results and discussion

PTDM design and synthesis

The presence of guanidinium groups and hydrophobic moieties in PTDs and PTDMs has previously been reported as crucial for protein delivery.[51] To investigate the role of hydrophobicity and charge density, a series of monomers with varying hydrophobic and cationic content was synthesized (Fig. 1). The hydrophobic magnitude of monomers in Fig. 1B was assessed using reverse phase HPLC. The di-methyl (**dMe**) monomer had the lowest retention time (13.8 minutes), whereas methyl-phenyl (**MePh**) had an intermediate retention time (27.5 minutes) and the di-phenyl monomer (**dPh**) had the longest retention time (35.9 minutes) (Fig. 1). These retention times indicate that the addition of phenyl groups to the monomer increases hydrophobic content and is thus translatable to the hydrophobic content of the polymers. Two guanidine containing monomers, methyl-guanidine (**MeG**) and di-guanidine (**dG**), were also designed in order to investigate the role of cationic density within the positively charged block of the polymers.

These difunctional monomers were polymerized by ROMP to yield low dispersity (*Đ*) oxanorbornene block copolymers. GPC traces showed a complete shift in the final diblock toward a higher molecular weight compared to the first block, illustrating controlled polymerization and efficient chain extension. All polymers had narrow *Đ* values (≤1.1) as determined by GPC, and a phenyl to guanidine ratio consistent with expectations, as determined by ^1H NMR spectroscopy, available in the ESI.†

A series of four block copolymers was created comprised of a first block with ten phenyl substituents and a second block with ten guanidine substituents. Within these samples,

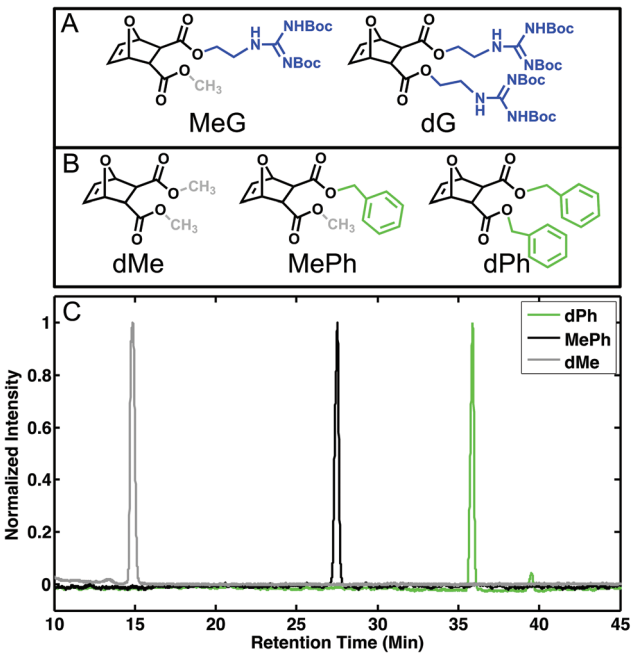

Fig. 1 Oxanorbornene monomers used in this study. (A) Guanidine containing monomers methyl guanidine (MeG) and di-guanidine (dG), with blue representing the cationic substituent and grey for the added methyl. (B) Hydrophobic monomers di-methyl (dMe), methyl-phenyl (MePh), and di-phenyl (dPh), with green representing the most hydrophobic components. (C) Reverse-phase HPLC chromatographs for dMe, MePh, and dPh monomers elucidating relative hydrophobicity.

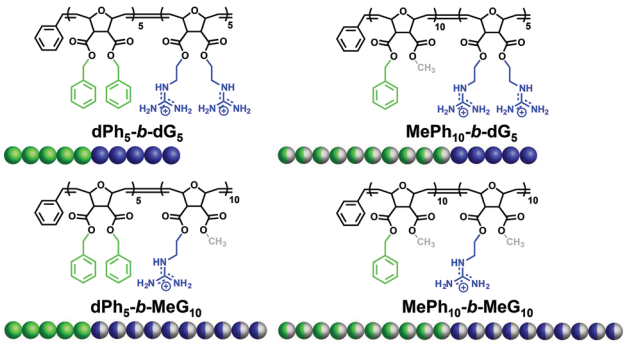

Fig. 2 Structures and cartoons of a polymer series with varying cationic and hydrophobic density. Each polymer contains 10 phenyl groups represented in green and 10 guanidinium groups represented in blue. The density of the hydrophobic and cationic groups is varied using a methyl substituent (grey).

however, the density of these functional groups is varied using the smallest methyl substituent to add space between hydrophobic or cationic groups. These are depicted in Fig. 2 as **dPh$_5$-*b*-dG$_5$**, **MePh$_{10}$-*b*-dG$_5$**, **dPh$_5$-*b*-MeG$_{10}$**, and **MePh$_{10}$-*b*-MeG$_{10}$**. This set of polymers was designed to explore the effect of varying charge and hydrophobic density along the polymer backbone on the ability of the PTDMs to deliver protein into HeLa, hTERT MSC, and Jurkat T cells.

To further investigate the effect of hydrophobic moieties and backbone contribution on protein delivery, the series was expanded to include another set of polymers that hold the high guanidinium density (**dG$_5$**) constant but vary hydrophobic density (either **dPh**, **MePh**, or **dMe**) and length (5 or 10) to compliment the initial polymer set. For example, **dPh$_{10}$-*b*-dG$_5$** has high hydrophobic density (**dPh**) with a length of ten to match the backbone length of the longest hydrophobic block (**MePh$_{10}$-*b*-dG$_5$**); **MePh$_5$-*b*-dG$_5$** was added to distinguish between added backbone length and decreased hydrophobic density (juxtapose **MePh$_{10}$-*b*-dG$_5$** and **dPh$_{10}$-*b*-dG$_5$**); lastly, **dMe$_5$-*b*-dG$_5$** and **dMe$_{10}$-*b*-dG$_5$** were included as controls to mimic the length of the backbone added by the hydrophobic blocks, while minimizing the hydrophobicity of the substituents. This second series of other polymers, displayed in Fig. 3, was specifically designed to decouple hydrophobic block length from hydrophobic content with respect to protein delivery.

DLS

Dynamic light scattering was performed on **dPh$_{10}$-*b*-dG$_5$**, **MePh$_{10}$-*b*-dG$_5$**, and **dMe$_{10}$-*b*-dG$_5$** to determine whether or not these molecules self-assemble in an aqueous environment (Fig. S1†). These three polymers were chosen to compare the maximum hydrophobic block lengths with varying phenyl group density. While this is not a direct indication of their ability to interact with cargo or transverse the membrane, it is important to understand whether they present a "hydrophobic core" in which the protein might reside or act as individual, solvated chains. **dMe$_{10}$-*b*-dG$_5$** had an R_h of 33 nm,

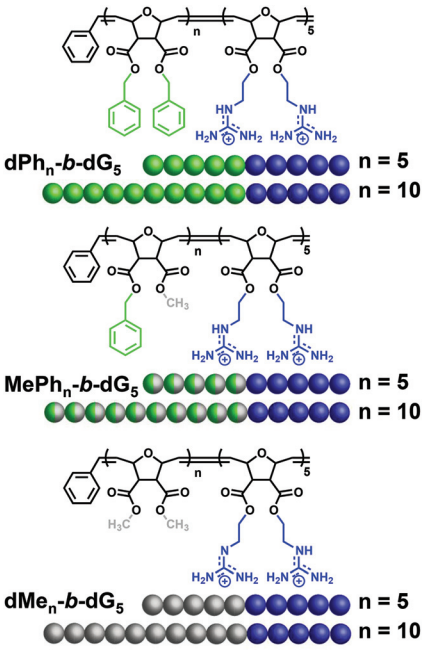

Fig. 3 Structures and cartoons of the second polymer series with varying hydrophobic density and length. **dPh$_5$-*b*-dG$_5$** and **MePh$_{10}$-*b*-dG$_5$** are repeated from Fig. 2 for ease of comparison. Hydrophobic phenyl substituents are represented in green, cationic moieties in blue, and methyl groups in grey.

MePh$_{10}$-*b*-dG$_5$ had an R_h value of 67 nm, and the relaxation curves for **dPh$_{10}$-*b*-dG$_5$** indicated a polydisperse R_h fit of 29 nm showing that all three block copolymers self assemble in aqueous solution. Given that the overall sizes are similar despite the variation in hydrophobic side chain suggests that the overall block architecture is more important for driving assembly than the side chain composition. Both polymers containing phenyl side chains had broader distributions, so it is possible that the side chains have some influence on the nanoparticles internal organization. Nevertheless, from these findings it can be hypothesized that the self-assembled aggregates provide a hydrophobic domain that allows the polymers to complex their cargo while the role of electrostatic interactions remains unclear given the phosphate buffer solution in which they are formed contains around 150 mM of salt.

Protein delivery

The ability of the polymers to facilitate the internalization of EGFP into cells was investigated in Jurkat T cells, HeLa cells, and hTERT MSCs. To assess protein delivery and viability, cells were analyzed using flow cytometry. In addition, confocal microscopy was used to image uptake into HeLa cells for the first series of polymers (Fig. 2). Trends were relatively consistent across the three cell lines with respect to their percent uptake, median fluorescence intensity (MFI), and viability profiles. While all polymers tested were able to deliver consistently into greater than 50% of the cell populations (ESI†), the amount of protein delivered, determined by MFI, varied based

on the polymer and, to a limited extent, cell type. Cell viability was above 95% in both HeLa and Jurkats, but slightly decreased to just above 80% for **dPh$_5$-*b*-dG$_5$** and **MePh$_{10}$-*b*-dG$_5$** in the hTERT MSCs as seen in ESI (Fig. S2†).

The MFI (Fig. 4) in all cell types, as established by flow cytometry, showed that **MePh$_{10}$-*b*-dG$_5$**, containing the high cationic density **dG** monomer, yielded greater internalization than its counterpart, **MePh$_{10}$-*b*-MeG$_{10}$**, with the **MeG** monomer. This indicates that increasing the cationic density of the block copolymer improves protein internalization, corroborating the suggestion that high guanidine density is important for membrane interactions and therefore delivery.[41] It should be noted that while there was no statistical difference between delivery using **dPh$_5$-*b*-dG$_5$** and **dPh$_5$-*b*-MeG$_{10}$**, the fluorescent shift appears higher for the more cationically dense polymer (**dPh$_5$-*b*-dG$_5$**) in Jurkats, suggesting that similar correlations could be drawn from this more sensitive cell line. These findings were additionally confirmed by images taken with CLSM of HeLa cells treated with the polymer–protein complexes, Fig. 5, which revealed both punctate and diffuse fluorescence within the cells.

While all four polymers yielded a complete shift in the fluorescence population of the cells, the MFI was 10× higher when using **MePh$_{10}$-*b*-dG$_5$** in all three cell types. Surprisingly, increasing hydrophobic density did not improve the ability of the polymers to deliver protein into any of the cell types, as seen by comparing **dPh$_5$-*b*-dG$_5$** with **MePh$_{10}$-*b*-dG$_5$**. With **MePh$_{10}$-*b*-dG$_5$**

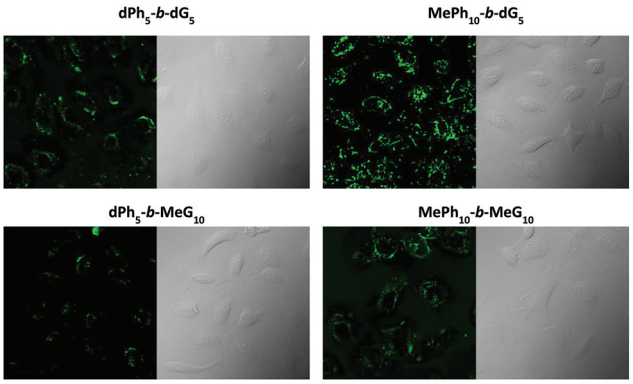

Fig. 5 CLSM images of EGFP delivery into HeLa cells by **MePh$_{10}$-*b*-MeG$_{10}$**, **MePh$_{10}$-*b*-dG$_5$**, **dPh$_5$-*b*-MeG$_{10}$**, and **dPh$_5$-*b*-dG$_5$**. Cells were treated with 2 μg of protein at a 20 : 1 polymer to protein ratio for 4 hours, and then washed 3 times to remove excess protein.

able to deliver the most protein (MFI ranging between 3000 to 4000) into the highest percentage of cells (around 95% depending on the cell type), high cationic density coupled with a lower density hydrophobic block appeared to optimize protein internalization. However, these comparisons alone do not fully decouple hydrophobic density of the monomer functional groups from potential hydrophobic effects related to the length. To explore this specific relationship, the series was expanded to

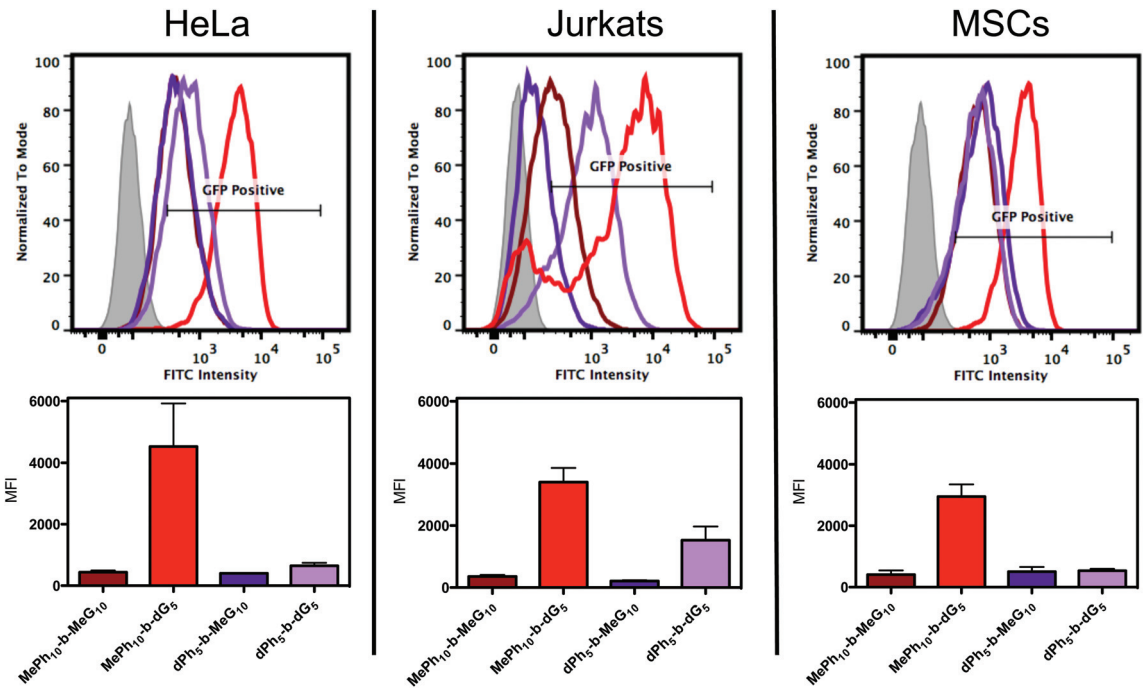

Fig. 4 Representative histograms (top) compared to a blank (grey) and the corresponding median fluorescence intensity (bottom) for EGFP delivery with **MePh$_{10}$-*b*-MeG$_{10}$**, **MePh$_{10}$-*b*-dG$_5$**, **dPh$_5$-*b*-MeG$_{10}$**, and **dPh$_5$-*b*-dG$_5$** into HeLa, Jurkat T cells, and hTERT MSCs. Cells were treated with 2 μg of protein at a 20 : 1 polymer to protein molar ratio for 4 hours, then washed with heparin to remove membrane bound proteins. A shift to the right from the grey blank in the histograms indicates higher fluorescence and was used to establish the median fluorescence intensity (MFI) as well as the percent uptake.

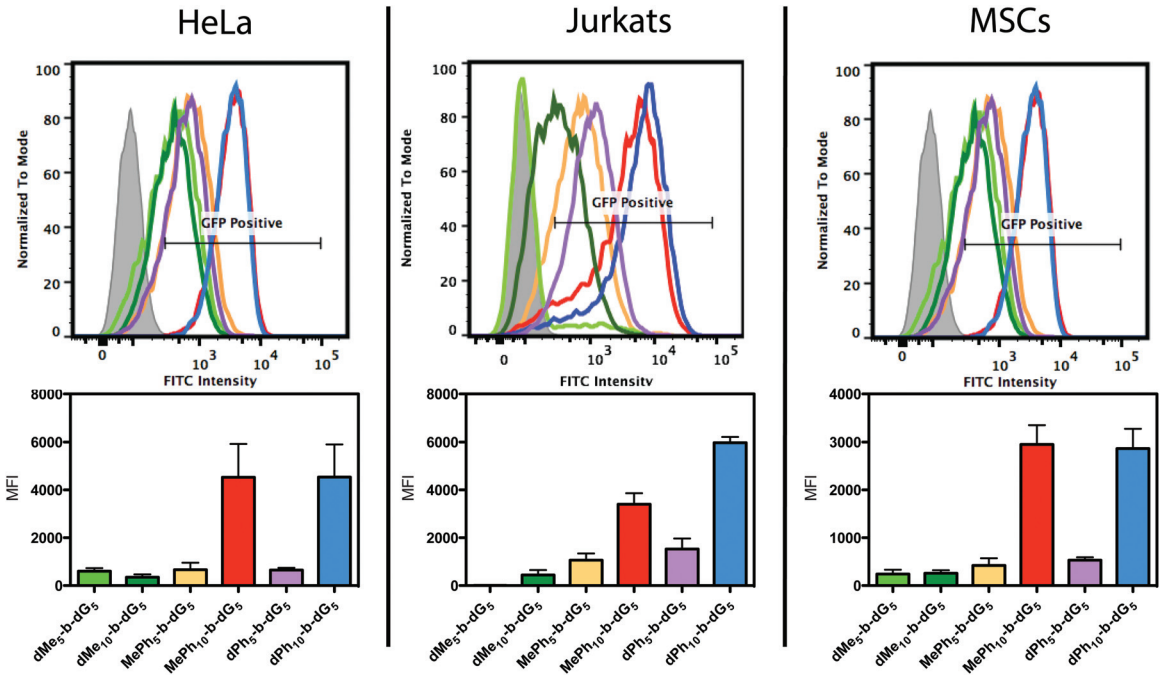

Fig. 6 Representative histograms and the corresponding median fluorescence intensity for EGFP delivery with **dMe$_5$-*b*-dG$_5$**, **dMe$_{10}$-*b*-dG$_5$**, **MePh$_5$-*b*-dG$_5$**, **MePh$_{10}$-*b*-dG$_5$**, **dPh$_5$-*b*-dG$_5$**, and **dPh$_{10}$-*b*-dG$_5$** into HeLa, Jurkat T cells, and hTERT MSCs. Cells were treated with 2 μg of protein at a 20 : 1 polymer to protein molar ratio for 4 hours, then washed with heparin to remove membrane bound proteins. A shift to the right from the grey blank in the histograms indicates higher fluorescence and was used to establish the median fluorescence intensity (MFI) as well as the percent uptake.

include **dPh$_{10}$-*b*-dG$_5$**, **MePh$_5$-*b*-dG$_5$**, **dMe$_5$-*b*-dG$_5$**, and **dMe$_{10}$-*b*-dG$_5$**, previously shown in Fig. 3.

These polymers all contain a cationic **dG** block length of 5, since high cationic density appears to be optimal for protein delivery. Higher internalization was seen when the **dPh** block length was increased from 5 to 10 (**dPh$_{10}$-*b*-dG$_5$**) yielding a higher MFI and effecting a higher percentage of the cell population in all cell types. Decreasing the **MePh** block length from 10 to 5 (**MePh$_5$-*b*-dG5**) reduced delivery and also the percentage of cells that received protein. More specifically, in Jurkats but not HeLa or the MSCs, there is an added advantage of using **dPh$_{10}$-*b*-dG$_5$** as it results in almost two fold higher MFI than **MePh$_{10}$-*b*-dG$_5$**. This difference highlights the tunability of this polymer platform to address specific cell types. Any additional hydrophobicity from the backbone, introduced by increasing the length of the polymer, was investigated by replacing the phenyl substituents with methyl groups (**dMe$_5$-*b*-dG$_5$** and **dMe$_{10}$-*b*-dG$_5$**). These polymers showed moderate protein delivery to a high number of cells, but the amount of protein delivered was far less than their phenyl containing counterparts (Fig. 6). This indicates that, in addition to increased block length, the presence of a threshold hydrophobicity is important for efficient cellular internalization of this cargo.

The ability to deliver proteins is substantially amplified when the hydrophobic block length is increased for the two phenyl-containing monomers (**MePh**, **dPh**), regardless of cell type. Both adherent cell types showed insignificant differences in MFI between **MePh$_{10}$-*b*-dG$_5$** and **dPh$_{10}$-*b*-dG$_5$**, while Jurkats were sensitive to the hydrophobic substituents with **dPh$_{10}$-*b*-dG$_5$** outperforming **MePh$_{10}$-*b*-dG$_5$**. Further investigation with other cell types, both adherent and suspension, might provide insight into this difference. Additionally, other polymer series with different hydrophobic substituents may help determine if the aromaticity of the phenyl group is indeed crucial, or cell type dependent. Lastly, optimization with different cargos would allow for further development and specificity of this polymer platform for increased internalization of proteins and antibodies into hard to transfect cell types.

Conclusion

Oxanorbornene block copolymers with varying cationic and hydrophobic density but the same charge and hydrophobic content were synthesized and characterized. While all of the PTDMs displayed the ability to deliver protein into HeLa, Jurkats, and hTERT MSCs, increased cationic density proved to have a slight edge over those with a methyl substituent on each guanidinium-based monomer. A second series of polymers highlighted the importance of hydrophobic length over density, although additional hydrophobicity from increasing the polymer backbone length does not exceed the hydrophobic threshold that is required for protein internalization. Increasing the length of the hydrophobic blocks may introduce better PTDM–protein interactions, facilitating delivery across the membrane. Further studies using different cargo types

such as intracellularly active proteins would highlight the capabilities of these block copolymers.

Acknowledgements

This work was primarily supported by NSF DMR-1308123. Supplemental funding from the NSF Eastern Asian and Pacific Summer Internship (EAPSI) fellowship program (grant IIA-1414767) and the Japanese Society for the Promotion of Science (JSPS) enabled collaboration with the Futaki laboratory at the University of Kyoto, Japan for microscope training and use. Joel Sarapas and Michael Kwasny are acknowledged for their contributions to the manuscript preparation. Additionally, authors also would like to thank Nick Posey for help with the HPLC. Authors would also like to acknowledge Amy Burnside and the University of Massachusetts Flow Core Facility.

References

1 J. P. Richard, K. Melikov, E. Vives, C. Ramos, B. Verbeure, M. J. Gait, L. V. Chernomordik and B. Lebleu, *J. Biol. Chem.*, 2003, **278**, 585–590.
2 F. Madani, S. Lindberg, U. Langel, S. Futaki and A. Gräslund, *J. Biophys.*, 2011, **2011**, 414729.
3 Y. S. Choi and A. E. David, *Curr. Pharm. Biotechnol.*, 2014, **15**, 192–199.
4 Y. S. Choi, J. Y. Lee, J. S. Suh, S. J. Lee, V. C. Yang, C. P. Chung and Y. J. Park, *Curr. Pharm. Biotechnol.*, 2011, **12**, 1166–1182.
5 M. Zorko and U. Langel, *Adv. Drug Delivery Rev.*, 2005, **57**, 529–545.
6 M. Green and P. M. Loewenstein, *Cell*, 1988, **55**, 1179–1188.
7 A. D. Frankel and C. O. Pabo, *Cell*, 1988, **55**, 1189–1193.
8 E. Vivès, P. Brodin and B. Lebleu, *J. Biol. Chem.*, 1997, **272**, 16010–16017.
9 J. B. Rothbard, T. C. Jessop, R. S. Lewis, B. A. Murray and P. A. Wender, *J. Am. Chem. Soc.*, 2004, **126**, 9506–9507.
10 D. J. Mitchell, D. T. Kim, L. Steinman, C. G. Fathman and J. B. Rothbard, *J. Pept. Res.*, 2000, **56**, 318–325.
11 P. A. Wender, D. J. Mitchell, K. Pattabiraman, E. T. Pelkey, L. Steinman and J. B. Rothbard, *Proc. Natl. Acad. Sci. U. S. A.*, 2000, **97**, 13003–13008.
12 E. Dupont, A. Prochiantz and A. Joliot, *J. Biol. Chem.*, 2007, **282**, 8994–9000.
13 D. Derossi, G. Chassaing and A. Prochiantz, *Trends Cell Biol.*, 1998, **8**, 84–87.
14 C. J. McKinlay, R. M. Waymouth and P. A. Wender, *J. Am. Chem. Soc.*, 2016, **138**, 3510–3517.
15 A. Joliot, C. Pernelle, H. Deagostini-Bazin and A. Prochiantz, *Proc. Natl. Acad. Sci. U. S. A.*, 1991, **88**, 1864–1868.
16 A. Elmquist, M. Lindgren, T. Bartfai and U. Langel, *Exp. Cell Res.*, 2001, **269**, 237–244.
17 S. Futaki, T. Suzuki, W. Ohashi, T. Yagami, S. Tanaka, K. Ueda and Y. Sugiura, *J. Biol. Chem.*, 2001, **276**, 5836–5840.
18 M. Pooga, M. Hällbrink, M. Zorko and U. Langel, *FASEB J.*, 1998, **12**, 67–77.
19 N. A. Alhakamy, P. Dhar and C. J. Berkland, *Mol. Pharm.*, 2016, **13**, 1047–1057.
20 S. Jones, J. Uusna, Ü. Langel and J. Howl, *Bioconjugate Chem.*, 2016, **27**, 121–129.
21 A. P. Blum, J. K. Kammeyer and N. C. Gianneschi, *Chem. Sci.*, 2016, **7**, 989–994.
22 G. Gasparini and S. Matile, *Chem. Commun.*, 2015, **51**, 17160–17162.
23 G. Gasparini, E.-K. K. Bang, J. Montenegro and S. Matile, *Chem. Commun.*, 2015, **51**, 10389–10402.
24 S. Katayama, H. Hirose, K. Takayama, I. Nakase and S. Futaki, *J. Controlled Release*, 2011, **149**, 29–35.
25 N. Sakai, T. Takeuchi, S. Futaki and S. Matile, *ChemBioChem*, 2005, **6**, 114–122.
26 T. Takeuchi, M. Kosuge, A. Tadokoro, Y. Sugiura, M. Nishi, M. Kawata, N. Sakai, S. Matile and S. Futaki, *ACS Chem. Biol.*, 2006, **1**, 299–303.
27 M. C. Morris, J. Depollier, J. Mery, F. Heitz and G. Divita, *Nat. Biotechnol.*, 2001, **19**, 1173–1176.
28 M. C. Morris, S. Deshayes, F. Heitz and G. Divita, *Biol. Cell*, 2008, **100**, 201–217.
29 S. Deshayes, M. C. Morris, G. Divita and F. Heitz, *J. Pept. Sci.*, 2006, **12**, 758–765.
30 W. C. Wimley and S. H. White, *Nat. Struct. Biol.*, 1996, **3**, 842–848.
31 D. Sengupta, J. C. Smith and G. M. Ullmann, *Biochim. Biophys. Acta*, 2008, **1778**, 2234–2243.
32 W. M. Yau, W. C. Wimley, K. Gawrisch and S. H. White, *Biochemistry*, 1998, **37**, 14713–14718.
33 F. Perret, M. Nishihara, T. Takeuchi, S. Futaki, A. N. Lazar, A. W. Coleman, N. Sakai and S. Matile, *J. Am. Chem. Soc.*, 2005, **127**, 1114–1115.
34 K. Witte, B. E. Olausson, A. Walrant, I. D. Alves and A. Vogel, *Biochim. Biophys. Acta*, 2013, **1828**, 824–833.
35 A. Walrant, I. Correia, C.-Y. Y. Jiao, O. Lequin, E. H. Bent, N. Goasdoué, C. Lacombe, G. Chassaing, S. Sagan and I. D. Alves, *Biochim. Biophys. Acta*, 2011, **1808**, 382–393.
36 K. Takayama, H. Hirose, G. Tanaka, S. Pujals, S. Katayama, I. Nakase and S. Futaki, *Mol. Pharm.*, 2012, **9**, 1222–1230.
37 I. Nakase, T. Takeuchi, G. Tanaka and S. Futaki, *Adv Drug Delivery Rev.*, 2008, **60**, 598–607.
38 P. A. Wender, W. C. Galliher, E. A. Goun, L. R. Jones and T. H. Pillow, *Adv Drug Delivery Rev.*, 2008, **60**, 452–472.
39 A. Hennig, G. J. Gabriel, G. N. Tew and S. Matile, *J. Am. Chem. Soc.*, 2008, **130**, 10338–10344.
40 A. Ö. Tezgel, G. Gonzalez-Perez, J. C. Telfer, B. A. Osborne, L. M. Minter and G. N. Tew, *Mol. Ther.*, 2013, **21**, 201–209.
41 A. Ö. Tezgel, J. C. Telfer and G. N. Tew, *Biomacromolecules*, 2011, **12**, 3078–3083.

42 A. Som, A. Reuter and G. N. Tew, *Angew. Chem., Int. Ed.*, 2012, **51**, 980–983.
43 B. M. deRonde, A. Birke and G. N. Tew, *Chem. – Eur. J.*, 2015, **21**, 3013–3019.
44 F. Sgolastra, C. M. Backlund, I. Ozay, B. M. deRonde, L. M. Minter and G. N. Tew, *J. Controlled Release*, (in review).
45 F. Sgolastra, L. M. Minter, B. A. Osborne and G. N. Tew, *Biomacromolecules*, 2014, **15**, 812–820.
46 K. Lienkamp, A. E. Madkour, K.-N. N. Kumar, K. Nüsslein and G. N. Tew, *Chem. – Eur. J.*, 2009, **15**, 11715–11722.
47 A. Som, A. O. Tezgel, G. J. Gabriel and G. N. Tew, *Angew. Chem., Int. Ed. Engl.*, 2011, **50**, 6147–6150.
48 A. Dinca, W.-M. M. Chien and M. T. Chin, *Int. J. Mol. Sci.*, 2016, **17**, 263.
49 M. Kristensen, D. Birch and H. Mørck Nielsen, *Int. J. Mol. Sci.*, 2016, **17**, 185.
50 A. Eguchi and S. F. Dowdy, *Trends Pharmacol. Sci.*, 2009, **30**, 341–345.
51 K. Takayama, I. Nakase, H. Michiue, T. Takeuchi, K. Tomizawa, H. Matsui and S. Futaki, *J. Controlled Release*, 2009, **138**, 128–133.